Mineralogical Magazine, August 2012, Vol. 76(4), pp. 933–948

The low-temperature behaviour of cancrinite: an *in situ* single-crystal X-ray diffraction study

G. Diego Gatta[1,2,*], P. Lotti[1], V. Kahlenberg[3] and U. Haefeker[3]

[1] Dipartimento di Scienze della Terra, Università degli Studi di Milano, Via Botticelli 23, I-20133 Milano, Italy
[2] CNR-Istituto per la Dinamica dei Processi Ambientali, Milano, Italy
[3] Institut für Mineralogie und Petrographie, Leopold Franzens Universität Innsbruck, Innrain 52, A - 6020 Innsbruck, Austria

[*Received 30 September 2011; Accepted 14 December 2011; Associate Editor: Roger Mitchell*]

ABSTRACT

The low-temperature structural behaviour of natural cancrinite with a formula $Na_{6.59}Ca_{0.93}[Si_{6.12}Al_{5.88}O_{24}](CO_3)_{1.04}F_{0.41}\cdot 2H_2O$ has been investigated by means of *in situ* single-crystal X-ray diffraction and Raman spectroscopy. High quality structure refinements were obtained at 293, 250, 220, 180, 140, 100 and at 293 K again (at the end of the low-*T* experiments). The variation in the unit-cell volume as a function of temperature (*T*) exhibits a continuous trend, without any evident thermoelastic anomaly. The thermal expansion coefficient $\alpha_V = (1/V)\partial V/\partial T$ is $3.8(7)\times 10^{-5}$ K^{-1} (between 100 and 293 K). The structure refinement based on intensity data collected at ambient conditions after the low-*T* experiment confirmed that the low-*T* induced deformation processes are completely reversible. The extraframework population does not show significant variations down to 100 K. The strong positional disorder of the carbonate groups along the *c* axis persists within the *T* range investigated. The structural behaviour of cancrinite at low-*T* is mainly governed by the continuous framework rearrangement through the ditrigonalization of the six-membered rings which lie in a plane perpendicular to [0001], the contraction of the four-membered ring joint units, the decrease of the ring corrugation in the (0001) plane, and the flattening of the cancrinite cages. A list of the principal Raman active modes in ambient conditions is provided and discussed.

Keywords: cancrinite, low temperature, single-crystal X-ray diffraction, structure refinement.

Introduction

Cancrinite, ideally $(Na,Ca)_{7-8}[Al_6Si_6O_{24}](CO_3)_{1.2-1.7}\cdot 2H_2O$, is a zeolite-like mineral which crystallizes as a primary phase in low-silica alkaline igneous rocks and also forms as an alteration product of nepheline. It is the parent of the homonymous mineral group (Bonaccorsi and Merlino, 2005; Cámara *et al.*, 2005, 2010; Rastvetaeva *et al.*, 2007), the most common members of which are cancrinite, davyne and vishnevite.

The crystal structure of cancrinite was first described by Pauling (1930) and refined by Jarchow (1965). The [CAN] framework consists of layers of interconnected six-membered rings perpendicular to [0001] (described hereafter 6mR⊥[0001]), close-packed according to an ...ABAB... stacking sequence (Fig. 1), with full (Al,Si)-tetrahedral ordering. Each ring is centred on the threefold axis and linked directly to 3 twelve-membered rings and to 3 + 3 six-membered rings by 4mR joint units, which produces double zigzag chains along [0001] (Figs 1 and 2). This structural scheme generates columns of base-sharing cages (Fig. 1), the so called cancrinite cages [or ε, or undecahedral cages; 4^66^5 according to the IUPAC

* E-mail: diego.gatta@unimi.it
DOI: 10.1180/minmag.2012.076.4.10

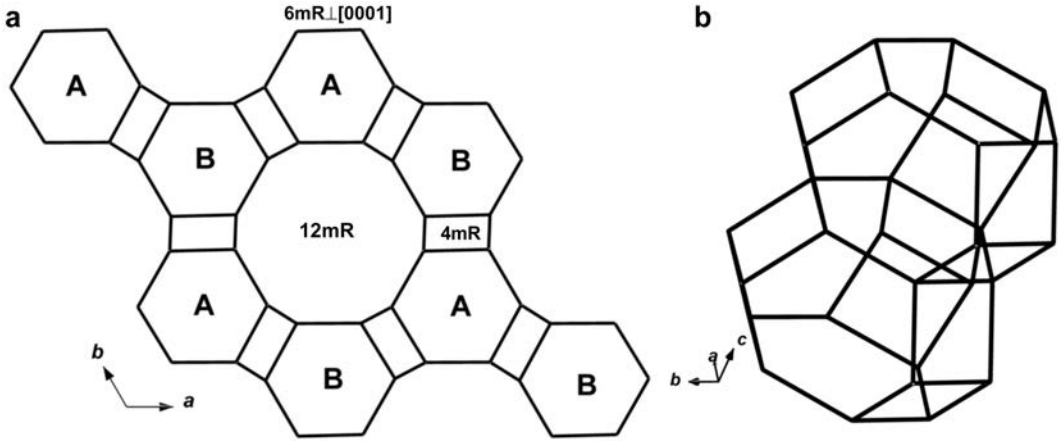

FIG. 1. (*a*) The structure of the cancrinite framework which consists of interconnected six-membered rings which lie in planes perpendicular to [0001], and which have an ...ABAB... stacking sequence. (*b*) Column of cancrinite cages.

recommendations, McCusker *et al.* (2001)], and parallel 12mR channels. Cages and channels are connected by 6-membered rings of tetrahedra approximately parallel to [0001] (hereafter 6mR∠[0001]) (Fig. 2). The topological symmetry of the [CAN] framework is $P6_3/mmc$ with lattice parameters a = 12.5 Å and c = 5.3 Å (Baerlocher *et al.*, 2007). However, the complete order of the (Al,Si) tetrahedra lowers the [CAN] symmetry to that of space group $P6_3$ (Jarchow, 1965).

Cancrinite voids are occupied by both cations and anions. The cages are filled by Na ions and H_2O molecules to produce $-Na-H_2O-$ $Na-H_2O-$ chains (Fig. 3). Davyne and microsommite contain $-Ca-Cl-Ca-Cl-$ chains with constant bond lengths (Bonaccorsi and Merlino, 2005). The H_2O oxygen lies off the triad axis, giving three mutually exclusive disordered positions (Jarchow, 1965; Grundy and Hassan, 1982) which are not coplanar with the hydrogen atoms; each hydrogen has two possible H-bonds with framework oxygen atoms (Della Ventura *et al.*, 2009). The iso-oriented channels have a 5.9 Å free diameter (Baerlocher *et al.*, 2007) and contain two mutually exclusive carbonate group sites in their centres, and Na cation sites near their

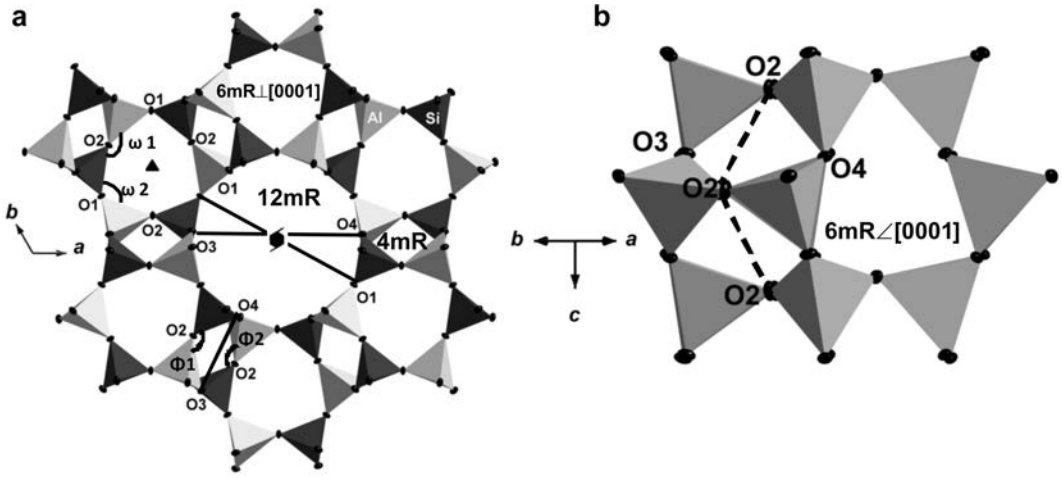

FIG. 2. (*a*) The cancrinite framework viewed down [0001]. The central channel (a 12mR) is surrounded by 6 columns of cancrinite cages. (*b*) The cancrinite cage. The κ angle (*O*2−*O*2−*O*2) is shown.

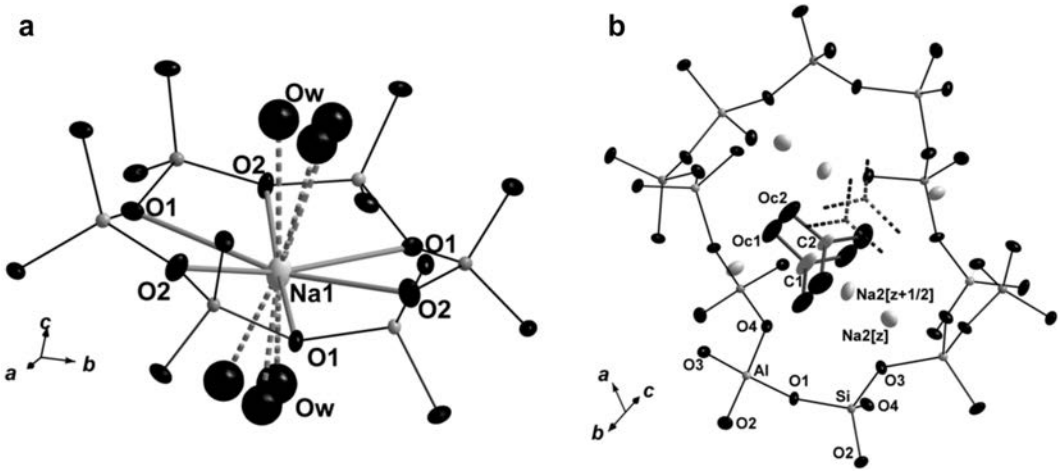

FIG. 3. (*a*) Configuration of the cancrinite cage content; dashed lines represent sets of three mutually exclusive *Na*1−*Ow* bonds. (*b*) The channel contents.

walls; the Na in the channels can be partially replaced by Ca. Structures with two mutually exclusive cation sites have been reported (Ballirano and Maras, 2005, and references therein). Other anions including SO_4^{2-}, NO_3^-, Cl^- and OH^-, and H_2O molecules can occupy the channel sites (Bresciani-Pahor *et al.*, 1982; Grundy and Hassan, 1982; Hassan and Grundy, 1984, 1991; Buhl *et al.*, 2000; Fechtelkord *et al.*, 2001). Cancrinite superstructures have been reported, due to the ordering of the CO_3 clusters and their vacancies in the channels (Brown and Cesbron, 1973; Foit *et al.*, 1973; Grundy and Hassan, 1982; Hassan and Buseck, 1982).

Several studies in the last decade have been devoted to potential uses of synthetic cancrinite. Cancrinite channels can be used, for example, as hosts for chains of Se_2^{2-} and Se_2^- dimers, to produce a material with optical properties that are of technological interest (Poborchii, 1994; Poborchii *et al.*, 2002). Crystalline NO_3-bearing cancrinite was found as a precipitation product in nuclear waste tanks at the Hanford site, Washington, USA and as product of the reaction between simulated leaked waste fluids and quartz- and kaolinite-bearing sediments at the same site (Bickmore *et al.*, 2001; Buck and McNamara, 2004; Zhao *et al.*, 2004). These precipitated crystals revealed a low sorption capacity for the Cs^+ ions present in the nuclear-waste fluids (Zhao *et al.*, 2004). Cancrinite is also the final product of Na-aluminosilicate precipitation from liquor during the Bayer process for the refining of bauxite for alumina production (Gerson and Zheng, 1997; Barnes *et al.*, 1999).

Hassan *et al.* (2006) studied the elastic and structural behaviour of a natural cancrinite up to 1255 K by means of X-ray powder diffraction. They reported a phase transition at about 777 K with loss of superstructure and a discontinuity in the unit-cell parameters. A continuous dehydration process was observed up to 898 K; above this temperature an anhydrous phase is formed. Only minimal loss of CO_2 was reported in the *T*-range investigated by Hassan *et al.* (2006), but the complete release of CO_2 has been reported at different temperatures in other cancrinite-like phases (Della Ventura *et al.*, 2007; Bonaccorsi *et al.*, 2007). A further *in situ* high temperature single-crystal diffraction study of a natural cancrinite was reported by Isupova *et al.* (2010) who reported a series of structure refinements at temperatures up to 673 K. The elastic behaviour and the pressure-induced structural behaviour of $Na_6Cs_2Ga_6Ge_6O_{24}{\cdot}Ge(OH)_6$, a synthetic compound isotypic with cancrinite, have been investigated up to 5 GPa by means of *in situ* X-ray synchrotron powder diffraction by Gatta and Lee (2008). No evidence of a phase transition was observed in the *P* range investigated.

To the best of our knowledge, the behaviour of cancrinite has not been studied at low temperature. The aim of this study is the investigation of the low-*T* behaviour of cancrinite by means of *in situ* single-crystal X-ray diffraction, in order to describe its thermoelastic properties, the main

deformation mechanisms and any effect of the temperature on carbonate group positional disorder (Grundy and Hassan, 1982; Della Ventura *et al.*, 2009). The low-*T* structure evolution mechanisms in cancrinite can be compared with those in response to high pressure (high-*P*), as an *in situ* high-pressure single-crystal X-ray diffraction study of cancrinite was performed (Lotti *et al.*, 2012). This allows a comparative analysis of the elastic behaviour and the main deformation mechanisms in 'compressive' regimes corresponding to high-pressure and low-temperature conditions. In addition, unpolarized Raman spectra (in the regions from 100 to 1400 cm^{-1} and 3400 to 3800 cm^{-1}) of the natural cancrinite used for the low-*T* diffraction experiment are provided and discussed, as a comprehensive assignment of the Raman active modes in these regions has not been reported.

Materials and experimental methods

A fragment of a centimetre-size gem-quality crystal of cancrinite from Cameroun [also used by Della Ventura *et al*. (2009)], which was free from defects at the optical scale, was selected for the X-ray diffraction experiments. The chemical formula of this cancrinite, reported by Della Ventura *et al*. (2009) by electron-microprobe analysis in wavelength-dispersive mode, is $Na_{6.59}Ca_{0.93}[Si_{6.12}Al_{5.88}O_{24}](CO_3)_{1.04}F_{0.41}\cdot 2H_2O$.

Intensity diffraction data were collected at 293, 250, 220, 180, 140, 100 and then again at 293 K using an Oxford Diffraction Gemini Ultra diffractometer, equipped with a Ruby CCD detector and graphite monochromator, operating at 50 kV and 40 mA with Mo*K*α radiation. Low temperature data collections were performed with the crystal cooled by an Oxford Cryosystems 700 series Plus open-flow nitrogen gas device (with a temperature stability of better than 0.2 K, and an absolute uncertainty within 2 K at the crystal position). A combination of ω and φ scans was used to maximize data coverage and redundancy, with 1º scan width, 29 s frame exposure time and maximum 2θ of ~80º. The crystal was found to be metrically hexagonal across the entire *T*-range investigated, with the following unit-cell parameters at ambient temperature and pressure: $a = b = 12.6018(3)$, $c = 5.1204(2)$ Å and $V = 704.21(2)$ Å^3. Systematic absences were compatible with space group $P6_3$ at all of the temperatures, and no evidence of superstructure or twinning was found. Lorentz-polarization corrections were applied to all the datasets using *Crysalis* software (Oxford Diffraction, 2008). Further details pertaining to the data collection strategies are given in Table 1.

Unpolarized single-crystal Raman spectra at room temperature were collected from the same crystal used for the low-*T* X-ray diffraction experiments, using a HORIBA Labram HR-800 confocal Raman spectrometer equipped with an open-electrode charge-coupled device (CCD) detector. The sample was excited with a Nd:YAG laser (30 mW, 532 nm). The laser beam was focussed through a 100× objective (N.A. = 0.9) to a 1 μm spot. The laser power at the sample surface was approximately 5 mW. The spectral regions from 100 to 1400 cm^{-1} and 3400 to 3800 cm^{-1} were investigated. Raman spectra were recorded in backscattered geometry for 2×200 s (Fig. 4) at a resolution of less than 2 cm^{-1}. A grating with 1800 lines mm^{-1} was used to disperse the scattered Raman light. The accuracy of Raman line positions is ~0.5 cm^{-1}; emission lines from a Ne lamp were used as a calibration.

Results

Thermoelastic behaviour

The low-*T* behaviour of the unit-cell volume of cancrinite is shown in Fig. 5. The cell volume decreases monotonically within the *T*-range investigated, and similar behaviour is also observed along the unit-cell edges. No evidence of a phase transition was found in the *T*-range investigated. The *V*–*T* data were fitted using the equation derived from the thermodynamic definition of the thermal expansion coefficient (α) (Fig. 5), $V(T) = V_{T0}\exp(\alpha\Delta T)$, where α is considered to be constant with *T*. The refined parameters are $\alpha_V = 3.8(7) \times 10^{-5}$ K^{-1} and $V_0 = 698.2(6)$ Å^3. The same protocol was applied to the *a vs. T* and *c vs. T* data, leading to the refined parameters $\alpha_a = 0.7(2) \times 10^{-5}$ K^{-1} with $a_0 = 12.580(3)$ Å; and $\alpha_c = 2.1(3) \times 10^{-5}$ K^{-1} with $c_0 = 5.096(2)$ Å, where α_a and α_c are the linear expansion coefficients. The mean thermal expansion coefficients between 293 and 100 K [$\bar{\alpha} = 1/x_0(\Delta x/\Delta T)$] were also calculated and are as follows: $\bar{\alpha}_V = 4.1(2) \times 10^{-5}$ K^{-1}, $\bar{\alpha}_a = 0.81(4) \times 10^{-5}$ K^{-1} and $\bar{\alpha}_c = 2.48(7) \times 10^{-5}$ K^{-1}.

As the unit cell *V* values at 140 and 100 K differ by less than 3σ (Table 1), we performed a further *V*–*T* fit excluding the data point at 100 K. The refined parameters are $\alpha_V = 5(1) \times 10^{-5}$ K^{-1} and $V_0 = 697(1)$ Å^3.

TABLE 1. Details of the structure refinements of cancrinite.

T (K)	293	250	220	180	140	100	293*
a (Å)	12.6018(3)	12.5885(3)	12.5887(3)	12.5827(3)	12.5792(5)	12.5821(2)	12.6013(4)
c (Å)	5.1204(2)	5.1091(1)	5.1110(1)	5.0998(2)	5.1003(2)	5.0960(1)	5.1205(2)
V (Å^3)	704.21(2)	701.17(4)	701.46(4)	699.25(4)	698.93(6)	698.66(3)	704.16(6)
Z	1	1	1	1	1	1	1
Maximum 2θ (º)	77.88	77.67	77.48	77.72	77.55	77.62	77.78
h range	$-22 \leqslant h \leqslant 14$	$-18 \leqslant h \leqslant 21$	$-19 \leqslant h \leqslant 21$	$-21 \leqslant h \leqslant 18$	$-22 \leqslant h \leqslant 15$	$-17 \leqslant h \leqslant 22$	$-20 \leqslant h \leqslant 22$
k range	$-18 \leqslant k \leqslant 21$	$-21 \leqslant k \leqslant 21$	$-21 \leqslant k \leqslant 18$	$-21 \leqslant k \leqslant 21$	$-20 \leqslant k \leqslant 21$	$-22 \leqslant k \leqslant 21$	$-21 \leqslant k \leqslant 15$
l range	$-8 \leqslant l \leqslant 8$	$-8 \leqslant l \leqslant 8$	$-8 \leqslant l \leqslant 8$	$-8 \leqslant l \leqslant 8$	$-8 \leqslant l \leqslant 8$	$-8 \leqslant l \leqslant 8$	$-9 \leqslant l \leqslant 8$
Measured reflections	11,305	10,843	11,277	10,761	11,203	11,670	11,235
Unique reflections	2617	2518	2596	2509	2596	2614	2572
Unique reflections, $F_0 > 4\sigma(F_0)$	2260	2187	2303	2222	2292	2318	2163
R_{int}	0.0407	0.0408	0.0422	0.0433	0.0446	0.0451	0.0486
Number of l.s. parameters	99	97	97	97	97	97	99
R_1, $F_0 > 4\sigma(F_0)$	0.0378	0.0362	0.0339	0.0346	0.0346	0.0348	0.0381
R_1, all data	0.0478	0.0468	0.0421	0.0435	0.0441	0.0419	0.0512
wR_2	0.0586	0.0584	0.0571	0.0570	0.0576	0.0579	0.0614
GooF	1.439	1.448	1.419	1.361	1.371	1.375	1.433
Residuals (e$^-$ Å^{-3})	+0.94/−0.67	+0.99/−0.68	+0.93/−0.75	+0.95/−0.73	+1.07/−0.82	+0.98/−0.73	+0.93/−0.70

* The final dataset collected after the cooling cycle.

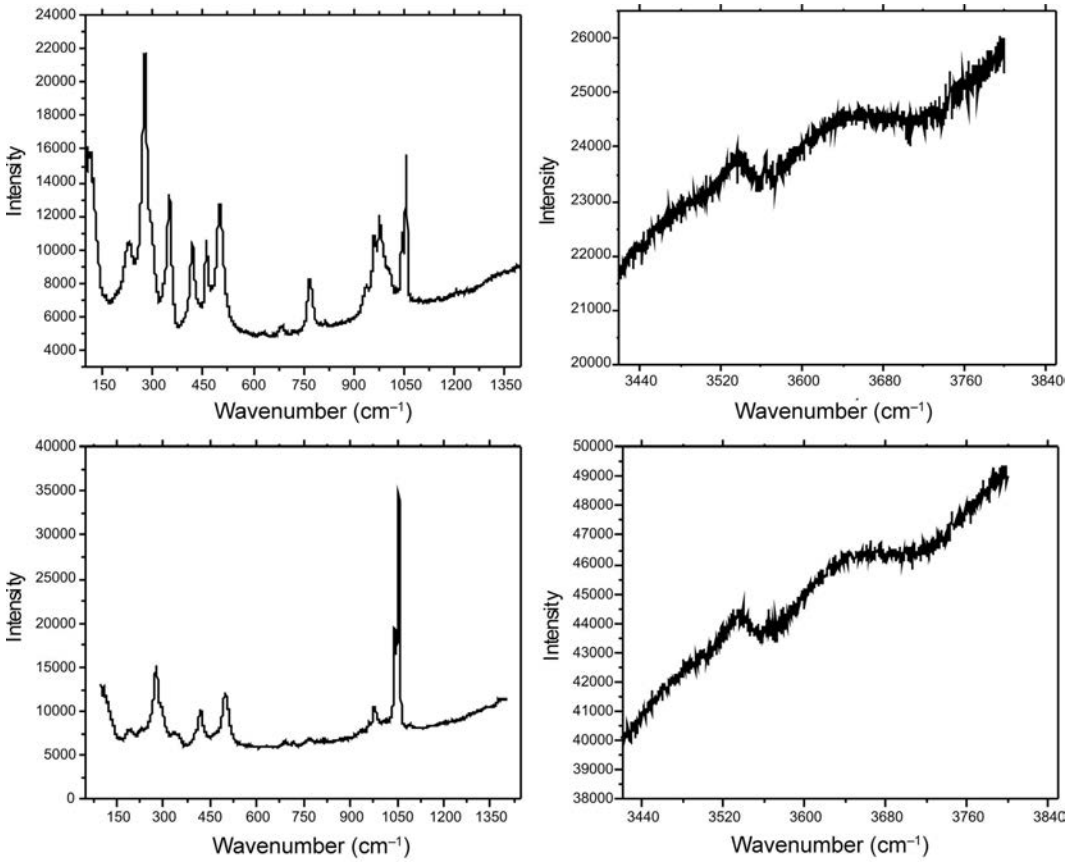

FIG. 4. Unpolarized single-crystal Raman spectra of cancrinite collected at room temperature in the regions 100−1400 and 3400−3800 cm^{-1} with the crystal in two different orientations (crystal rotated by 90º). The list of the frequencies of the main Raman bands is given in Table 5. None of the spectra are corrected for background.

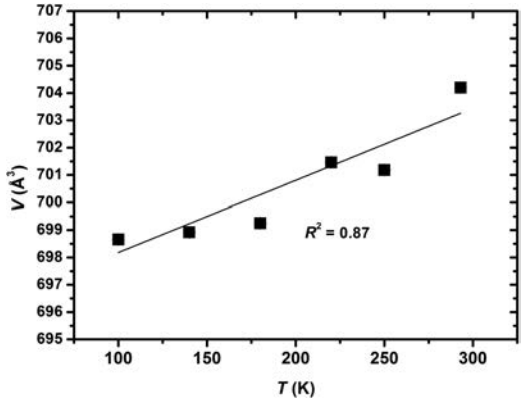

FIG. 5. The unit-cell volume of cancrinite as a function of T. The solid line represents the $V-T$ fit using the equation $V(T) = V(T_0)\exp(\alpha\Delta T)$.

Structure refinements

The structure refinement based on X-ray diffraction intensity data collected at 293 K was performed with the *SHELXL-97* program (Sheldrick, 1997), using the atomic coordinates of Della Ventura *et al.* (2009) as starting model. Neutral atom scattering factors for Si, Al, Na, Ca, C and O from the *International Tables of Crystallography* (Wilson and Prince, 1999) were used. The C−O bond distances were restrained to be 1.300±0.005 Å, according to the refined values of Della Ventura *et al.* (2009). Hydrogen positions were not refined. The first cycles were performed with isotropic thermal displacement parameters and at a later stage the displacement parameters refined anisotropically. Only the *Ow* site was kept isotropic. The structure refinement (99 refined parameters) converged to an agree-

ment factor R_1 of 0.0378, based on 2260 intensity data with $F_o > 4\sigma(F_o)$, with no significant correlation in the variance-covariance matrix and residual peaks in the difference-Fourier density map of +0.94/−0.67 e^- $Å^{-3}$ (Table 1). Atom coordinates, occupancies and displacement parameters are listed in Table 2.

The refined extraframework sites confirmed the model previously described: a sodium-rich site (*Na*1, 2*b* Wyckoff position) in the cancrinite cage (Table 2), along with three mutually exclusive and symmetrically related H_2O oxygen sites (*Ow*), off the threefold axis (Fig. 3); the large channels are filled by a cationic site (*Na*2) occupied by Na (86.9(5)%) and Ca (13.1(5)%) (Table 2) in a general 6*c* position and by two mutually exclusive carbonate sites (with occupancies of 35(1)% and 47(1)%, respectively, Table 2), with the C sites (*C*1 and *C*2) in the centre of the channel on 2*a* special positions (1.25 Å apart on the 6_3 axis), and oxygen atoms on 6*c* general positions (*Oc*1 and *Oc*2 sites) (Fig. 3; Table 2).

The structure refinements at 250, 220, 180, 140 and 100 K were performed using the same strategy described above and constraining all the site-occupancy factors (s.o.fs) to the values refined at 293 K, except for the two carbonate groups (*C*1−*Oc*1 and *C*2−*Oc*2 sites). All refinements achieved convergence with no significant correlation in the variance-covariance matrix of the refined parameters or residual peaks in the difference-Fourier density maps. No change of the extraframework population was detected (e.g. site migration or ordering) in the *T*-range investigated. Further details pertaining to the structure refinements are listed in Table 1. Atom coordinates, site occupancies and U_{iso}/U_{eq} displacement parameters are given in Table 2. A table with the anisotropic displacement parameters has been deposited with *Mineralogical Magazine* and is available at www.minersoc.org/pages/e_journals/dep_mat.html.

Test refinements were performed for the low-*T* datasets leaving the *Ow* s.o.f. free, in order to detect any potential N_2-flux induced dehydration phenomena (Gatta and Lotti, 2011). However, no significant change of the s.o.f. value was detected. A structure refinement based on the intensity data collected at room-*T* after the low-*T* experiments was also performed, showing that any low-*T* induced structure modification is completely reversible (Tables 1 and 2).

Low-T framework behaviour

The 6mR⊥[0001] units show a 'ditrigonalization process' with decreasing temperature, as shown by the opening of the ω1 angle (*O*1−*O*2−*O*1) and the closure of the ω2 angle (*O*2−*O*1−*O*2) (Fig. 2; Table 3), and described by the 'ditrigonal rotation angle' α (Fig. 6; Table 3) [$\alpha = \frac{1}{6}\sum_i(|120^o - \theta_i|)/2$, where the θ_i are the angles between the basal edges of neighbouring tetrahedra articulated in the six-membered rings (Brigatti and Guggenheim, 2002)]. The 4mR joint units show a shortening along the *O*3−*O*4 distances coupled with the closure of the ψ1 (*O*3−*O*2′−*O*4) and ψ2 (*O*3−*O*2″−*O*4) angles (Figs 2 and 6, Table 3).

The channels size is controlled by the 12mR distances *O*1−*O*1, which shorten with decreasing

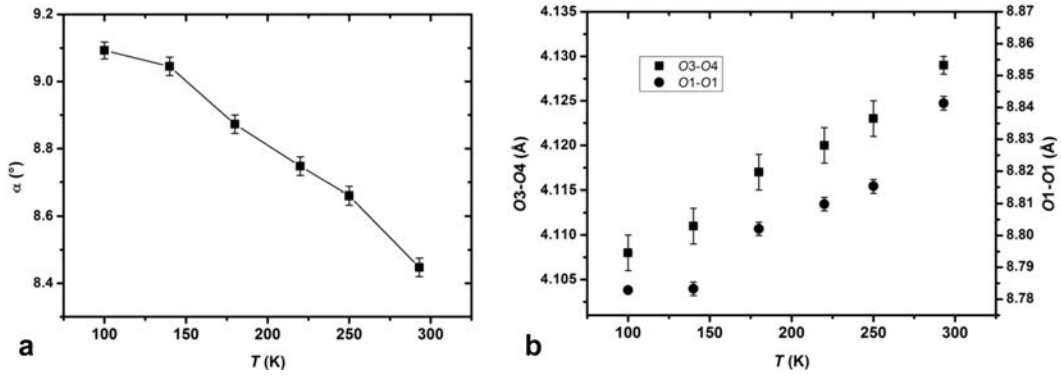

FIG. 6. (*a*) The change in the "ditrigonal rotation angle" (α) of the 6mR⊥[0001] as a function of *T*. (*b*) The change in the *O*3−*O*4 distance of the 4mR joint units and of the *O*1−*O*1 distance of 12mRs as a function of temperature.

TABLE 2. Refined atom coordinates and displacement parameters of cancrinite at 293, 250, 220, 180, 140, 100 and 293 K after the low-temperature experiment. The *Ow* site was refined with isotropic thermal displacement parameters.

T (K)	Site	Occupancy	*x/a*	*y/b*	*z/c*	U_{iso}/U_{eq}
293	*Si*	1.0	0.08266(3)	0.41076(3)	0.73332(8)	0.00694(6)
	Al	1.0	0.33706(3)	0.41216(3)	0.7342(1)	0.00695(7)
	*O*1	1.0	0.20182(9)	0.4050(1)	0.6425(2)	0.0139(2)
	*O*2	1.0	0.1145(1)	0.55067(9)	0.7108(3)	0.0187(2)
	*O*3	1.0	0.0444(1)	0.3589(1)	0.0278(2)	0.0148(2)
	*O*4	1.0	0.3210(1)	0.3509(1)	0.0450(2)	0.0144(2)
	*Na*1	0.957(6)	⅔	⅓	0.1177(3)	0.0275(5)
	*Na*2	0.894(4)	0.87422(5)	0.75144(6)	0.7765(1)	0.0246(3)
	*Ca*2	0.106(4)	0.87422(5)	0.75144(6)	0.7765(1)	0.0246(3)
	*C*1	0.345(9)	0	0	0.893(3)	0.032(3)
	*Oc*1	0.345(9)	0.0601(5)	0.1189(3)	0.880(2)	0.050(3)
	*C*2	0.472(9)	0	0	0.649 (3)	0.055(4)
	*Oc*2	0.472(9)	0.0616(3)	0.1193(3)	0.658(2)	0.052(2)
	Ow	⅓	0.3148(5)	0.6177(4)	0.168(1)	0.049(2)
250	*Si*	1.0	0.08271(3)	0.41078(3)	0.73328(8)	0.00602(6)
	Al	1.0	0.33708(3)	0.41223(3)	0.73431(9)	0.00606(7)
	*O*1	1.0	0.20144(9)	0.4043(1)	0.6410(2)	0.0120(2)
	*O*2	1.0	0.1150(1)	0.55100(9)	0.7102(3)	0.0167(2)
	*O*3	1.0	0.0447(1)	0.3592(1)	0.0285(2)	0.0135(2)
	*O*4	1.0	0.3208(1)	0.3511(1)	0.0455(2)	0.0127(2)
	*Na*1	0.957(6)	⅔	⅓	0.1172(3)	0.0227(3)
	*Na*2	0.894(4)	0.87411(5)	0.75142(6)	0.7768(1)	0.0223(2)
	*Ca*2	0.106(4)	0.87411(5)	0.75142(6)	0.7768(1)	0.0223(2)
	*C*1	0.36(1)	0	0	0.892(3)	0.030(3)
	*Oc*1	0.36(1)	0.0608(5)	0.1193(3)	0.878(2)	0.053(3)
	*C*2	0.46(2)	0	0	0.654(3)	0.055(5)
	*Oc*2	0.46(2)	0.0614(3)	0.1198(3)	0.657(2)	0.048(2)
	Ow	⅓	0.3143(5)	0.6165(4)	0.168(1)	0.043(1)
220	*Si*	1.0	0.08273(3)	0.41081(3)	0.73330(7)	0.00567(6)
	Al	1.0	0.33701(3)	0.41223(3)	0.73421(8)	0.00568(6)
	*O*1	1.0	0.20117(9)	0.40403(10)	0.6402(2)	0.0113(2)
	*O*2	1.0	0.1151(1)	0.55111(9)	0.7092(2)	0.0157(2)
	*O*3	1.0	0.0452(1)	0.3595(1)	0.0288(2)	0.0126(2)
	*O*4	1.0	0.3207(1)	0.3516(1)	0.0465(2)	0.0120(2)
	*Na*1	0.957(6)	⅔	⅓	0.1170 (3)	0.0204(3)
	*Na*2	0.894(4)	0.87414(5)	0.75131(6)	0.7766(1)	0.0211(1)
	*Ca*2	0.106(4)	0.87414(5)	0.75131(6)	0.7766(1)	0.0211(1)
	*C*1	0.349(9)	0	0	0.892(3)	0.029(3)
	*Oc*1	0.349(9)	0.0604(4)	0.1195(3)	0.882(2)	0.046(2)
	*C*2	0.480(8)	0	0	0.656(3)	0.057(4)
	*Oc*2	0.480(8)	0.0616(3)	0.1196(3)	0.660(2)	0.048(2)
	Ow	⅓	0.3139(5)	0.6157(4)	0.1673(9)	0.038(1)
180	*Si*	1.0	0.08277(3)	0.41074(3)	0.73330(8)	0.00509(6)
	Al	1.0	0.33699(3)	0.41216(3)	0.73423(9)	0.00510(7)
	*O*1	1.0	0.20122(9)	0.4039(1)	0.6392(2)	0.0102(2)
	*O*2	1.0	0.1156(1)	0.55122(8)	0.7086(2)	0.0142(2)
	*O*3	1.0	0.04549(9)	0.3598(1)	0.0301(2)	0.0117(2)
	*O*4	1.0	0.3206(1)	0.3517(1)	0.0471(2)	0.0109(2)
	*Na*1	0.957(6)	⅔	⅓	0.1155(3)	0.0171(2)
	*Na*2	0.894(4)	0.87426(5)	0.75151(5)	0.7765(1)	0.0191(1)
	*Ca*2	0.106(4)	0.87426(5)	0.75151(5)	0.7765(1)	0.0191(1)
	*C*1	0.384(9)	0	0	0.897(3)	0.036(3)
	*Oc*1	0.384(9)	0.0598(4)	0.1193(3)	0.882(2)	0.050(2)
	*C*2	0.447(9)	0	0	0.646(3)	0.047(4)
	*Oc*2	0.447(9)	0.0617(3)	0.1197(3)	0.657(1)	0.043(2)
	Ow	⅓	0.3131(4)	0.6153(3)	0.163(1)	0.034(1)

T (K)	Site	Occupancy	x/a	y/b	z/c	U_{iso}/U_{eq}
140	*Si*	1.0	0.08282(3)	0.41073(3)	0.73337(8)	0.00456(6)
	Al	1.0	0.33696(3)	0.41221(3)	0.73425(9)	0.00452(7)
	*O*1	1.0	0.20081(9)	0.4031(1)	0.6383(2)	0.0095(2)
	*O*2	1.0	0.1158(1)	0.55134(8)	0.7082(2)	0.0129(2)
	*O*3	1.0	0.0459(1)	0.3603(1)	0.0304(2)	0.0106(2)
	*O*4	1.0	0.3204(1)	0.3519(1)	0.0474(2)	0.0100(2)
	*Na*1	0.957(6)	⅔	⅓	0.1156(3)	0.0146(2)
	*Na*2	0.894(4)	0.87428(5)	0.75139(5)	0.7763(1)	0.0173(1)
	*Ca*2	0.106(4)	0.87428(5)	0.75139(5)	0.7763(1)	0.0173(1)
	*C*1	0.325(8)	0	0	0.894(3)	0.025(3)
	*Oc*1	0.325(8)	0.0602(4)	0.1194(3)	0.883(2)	0.037(2)
	*C*2	0.501(9)	0	0	0.659(3)	0.056(4)
	*Oc*2	0.501(9)	0.0620(3)	0.1203(3)	0.659(1)	0.047(2)
	Ow	⅓	0.3128(4)	0.6135(3)	0.1666(8)	0.028(1)
100	*Si*	1.0	0.08284(3)	0.41078(3)	0.73323(8)	0.00408(6)
	Al	1.0	0.33696(3)	0.41222(3)	0.73433(9)	0.00404(7)
	*O*1	1.0	0.20081(9)	0.40302(9)	0.6379(2)	0.0087(2)
	*O*2	1.0	0.11593(9)	0.55152(8)	0.7072(2)	0.0120(2)
	*O*3	1.0	0.04640(9)	0.3606(1)	0.0307(2)	0.0100(2)
	*O*4	1.0	0.32062(9)	0.3523(1)	0.0480(2)	0.0093(2)
	*Na*1	0.957(6)	⅔	⅓	0.1152(2)	0.0119(2)
	*Na*2	0.894(4)	0.87431(5)	0.75147(5)	0.7765(1)	0.0159(1)
	*Ca*2	0.106(4)	0.87431(5)	0.75147(5)	0.7765(1)	0.0159(1)
	*C*1	0.348(8)	0	0	0.894(3)	0.026(3)
	*Oc*1	0.348(8)	0.0606(4)	0.1196(3)	0.884(2)	0.039(2)
	*C*2	0.475(8)	0	0	0.658(3)	0.056(4)
	*Oc*2	0.475(8)	0.0616(3)	0.1199(2)	0.662(1)	0.044(2)
	Ow	⅓	0.3120(4)	0.6125(3)	0.1668(8)	0.0232(8)
293*	*Si*	1.0	0.08265(3)	0.41077(3)	0.7335(1)	0.00682(7)
	Al	1.0	0.33712(3)	0.41216(3)	0.7344(1)	0.00692(8)
	*O*1	1.0	0.2016(1)	0.4048(1)	0.6422(3)	0.0137(2)
	*O*2	1.0	0.1146(1)	0.55073(9)	0.7098(3)	0.0184(3)
	*O*3	1.0	0.0444(1)	0.3591(1)	0.0277(2)	0.0148(2)
	*O*4	1.0	0.3211(1)	0.3509(1)	0.0447(2)	0.0139(2)
	*Na*1	0.957(6)	⅔	⅓	0.1176(4)	0.0272(5)
	*Na*2	0.894(4)	0.87408(6)	0.75135(6)	0.7764(2)	0.0251(3)
	*Ca*2	0.106(4)	0.87408(6)	0.75135(6)	0.7764(2)	0.0251(3)
	*C*1	0.37(1)	0	0	0.896(3)	0.030(3)
	*Oc*1	0.37(1)	0.0603(5)	0.1190(3)	0.879(3)	0.055(4)
	*C*2	0.47(1)	0	0	0.651(4)	0.052(4)
	*Oc*2	0.47(1)	0.0616(4)	0.1195(3)	0.659(2)	0.053(3)
	Ow	⅓	0.3147(6)	0.6162(4)	0.169(1)	0.054(2)

* These data were collected after the low-T experiment.

temperature (Figs 2 and 6; Table 3), and the $O3-O4$ distances (Fig. 2; Table 3), which are almost constant within the temperature range investigated. The cancrinite cages flatten with decreasing temperature, a process that is described by the closure of the κ angle ($O2-O2-O2$) (Fig. 2). In each plane (A or B) of the 6mRs, a decrease of the 'corrugation' [defined as $\Delta z = c[z(O)_{max} - z(O)_{min}]$, where $z(O)_{max}$ is the maximum z coordinate of the oxygen belonging to the rings, $z(O)_{min}$ the minimum coordinate and c is the unit-cell edge length (Brigatti and Guggenheim, 2002)] with decreasing temperature is observed, along with the ditrigonalization of the rings (Fig. 7; Table 3). An increase of the ditrigonal shape is also shown by the 6mR⊿[0001] windows connecting channels and cages. The equivalent thermal parameters of the Si, Al and O sites decrease with decreasing temperature (Table 2).

TABLE 3. Relevant bond distances (Å) and angles (°), 6mR⊥[0001] ditrigonal rotation angle α (°) and corrugation (Å) at 293, 250, 220, 180, 140, 100 and 293 K after the low temperature experiment.

	T	293 K	250 K	220 K	180 K	140 K	100 K	293 K*
Si−	*O*1	1.608(1)	1.608(1)	1.608(1)	1.609(1)	1.609(1)	1.611(1)	1.607(1)
	*O*2	1.605(1)	1.606(1)	1.607(1)	1.607(1)	1.607(1)	1.609(1)	1.605(1)
	*O*3	1.618(1)	1.617(1)	1.618(1)	1.619(1)	1.618(1)	1.618(1)	1.616(1)
	*O*4	1.617(1)	1.618(1)	1.619(1)	1.618(1)	1.620(1)	1.618(1)	1.618(1)
<*Si–O*>		**1.612(1)**	**1.612(1)**	**1.613(1)**	**1.613(1)**	**1.614(1)**	**1.614(1)**	**1.612(1)**
Al−	*O*1	1.726(1)	1.727(1)	1.729(1)	1.728(1)	1.729(1)	1.730(1)	1.729(1)
	*O*2	1.722(1)	1.720(1)	1.720(1)	1.723(1)	1.723(1)	1.723(1)	1.722(1)
	*O*3	1.745(1)	1.744(1)	1.747(1)	1.742(1)	1.744(1)	1.747(1)	1.745(1)
	*O*4	1.736(1)	1.733(1)	1.737(1)	1.735(1)	1.735(1)	1.735(1)	1.734(1)
<*Al–O*>		**1.732(1)**	**1.731(1)**	**1.733(1)**	**1.732(1)**	**1.733(1)**	**1.734(1)**	**1.733(1)**
*Na*1−	*O*1(×3)	2.858(1)	2.863(1)	2.866(1)	2.866(1)	2.873(1)	2.875(1)	2.860(1)
	*O*2(×3)	2.437(1)	2.429(1)	2.427(1)	2.421(1)	2.418(1)	2.416(1)	2.435(1)
	Ow′	2.364(6)	2.359(6)	2.366(5)	2.377(5)	2.364(4)	2.361(4)	2.364(7)
	Ow″	2.870(6)	2.869(6)	2.868(5)	2.847(5)	2.870(4)	2.873(4)	2.878(7)
*Na*2/*Ca*2−	*O*1	2.535(1)	2.519(1)	2.514(1)	2.508(1)	2.499(1)	2.495(1)	2.533(2)
	*O*3′	2.457(1)	2.453(1)	2.449(1)	2.444(1)	2.442(1)	2.441(1)	2.458(1)
	*O*4′	2.439(1)	2.432(1)	2.429(1)	2.425(1)	2.422(1)	2.423(1)	2.438(1)
	*O*3″	2.922(1)	2.921(1)	2.927(1)	2.931(1)	2.937(1)	2.942(1)	2.922(1)
	*O*4″	2.891(1)	2.893(1)	2.899(1)	2.900(1)	2.903(1)	2.907(1)	2.892(1)
	*Oc*1′	2.474(9)	2.476(9)	2.461(7)	2.457(8)	2.449(7)	2.445(7)	2.48(1)
	*Oc*1″	2.408(4)	2.409(4)	2.409(4)	2.400(4)	2.407(4)	2.409(4)	2.409(5)
	*Oc*1‴	2.411(5)	2.400(5)	2.410(4)	2.413(4)	2.411(4)	2.408(4)	2.408(5)
	*Oc*2′	2.411(7)	2.395(7)	2.411(5)	2.395(6)	2.401(5)	2.412(6)	2.413(9)
	*Oc*2″	2.442(4)	2.435(4)	2.437(3)	2.437(4)	2.434(3)	2.429(4)	2.439(4)
	*Oc*2‴	2.412(4)	2.418(4)	2.411(4)	2.409(4)	2.407(3)	2.406(4)	2.414(4)
*Na*2/*Ca*2−	*C*1	2.778(4)	2.773(3)	2.774(3)	2.777(4)	2.775(3)	2.774(3)	2.781(4)
	*C*2	2.791(4)	2.781(4)	2.781(3)	2.789(4)	2.774(4)	2.775(4)	2.788(4)
ω1 (*O*1−*O*2−*O*1)		135.06(5)	135.43(5)	135.61(5)	135.84(5)	136.16(5)	136.29(5)	135.20(6)
ω2 (*O*2−*O*1−*O*2)		101.27(6)	100.79(6)	100.62(6)	100.35(6)	99.98(6)	99.92(5)	101.19(6)
*O*3−*O*4 (4mR)		4.129(3)	4.123(2)	4.120(2)	4.117(2)	4.111(2)	4.108(2)	4.127(2)
ψ1 (*O*3−*O*2′−*O*4)		95.31(6)	95.14(6)	95.02(6)	94.92(5)	94.72(5)	94.65(5)	95.32(6)
ψ2 (*O*3−*O*2″−*O*4)		95.65(6)	95.51(6)	95.27(5)	95.08(5)	94.93(5)	94.75(5)	95.49(6)
*O*1−*O*1 (12mR)		8.841(2)	8.815(2)	8.810(2)	8.802(2)	8.783(2)	8.783(1)	8.837(2)
*O*3−*O*4 (12mR)		8.486(1)	8.471(1)	8.475(1)	8.472(1)	8.474(1)	8.480(1)	8.481(1)
α		8.45(3)	8.66(3)	8.75(3)	8.87(3)	9.05(3)	9.09(3)	8.50(3)
Δ*z*		0.937(3)	0.928(3)	0.922(2)	0.910(2)	0.907(2)	0.899(2)	0.932(3)

* These data were collected after the low-*T* experiment.

Low-T extraframework behaviour

The equivalent displacement parameters of the *Na*1 and *Na*2 sites show a linear reduction with decreasing temperature (Fig. 8), and similar behaviour is observed also for the *Ow* site. In contrast, the equivalent displacement parameters of the carbonate group sites (i.e. *C*1, *Oc*1, *C*2, *Oc*2) remain almost constant within the temperature range investigated (Table 2).

The coordination polyhedron of the *Na*1 site lying in the cancrinite cage is a bipyramid with a ditrigonal base (corresponding to the 6mR⊥[0001] oxygen sites) and two H_2O oxygen atoms at the apical vertices; it has a coordination number (CN) of 8 (Fig. 3). Its

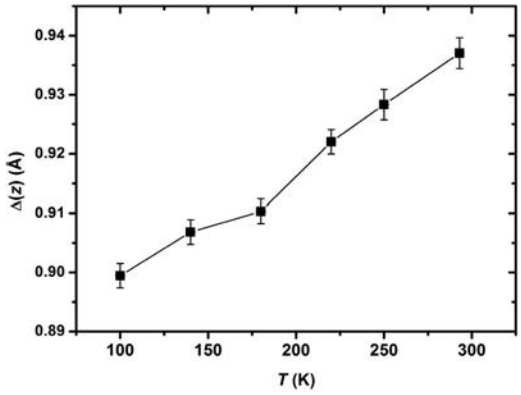

FIG. 7. The variation in the corrugation parameter of the rings in the (0001) plane, defined as $\Delta z = c[z(O)_{max} - z(O)_{min}]$ (see text for further details) as a function of temperature.

deformation is strictly controlled by the ditrigonalization of the rings, which leads to a shortening of the three *Na*1−*O*2 bond distances and to the stretching of the three *Na*1−*O*1 bonds, whereas the two independent *Na*1−*Ow* bond distances do not show any significant change with temperature (Table 3).

The *Na*2 site (i.e. the mixed Na/Ca site) is coordinated by five framework oxygen atoms and up to three carbonate oxygen atoms (maximum CN = 8) (Fig. 9). In each asymmetric unit (periodicity = *c*/2), two mutually exclusive sites, partially occupied by carbonate groups, were refined. Each asymmetric unit is therefore occupied by one CO_3 group, and there are three

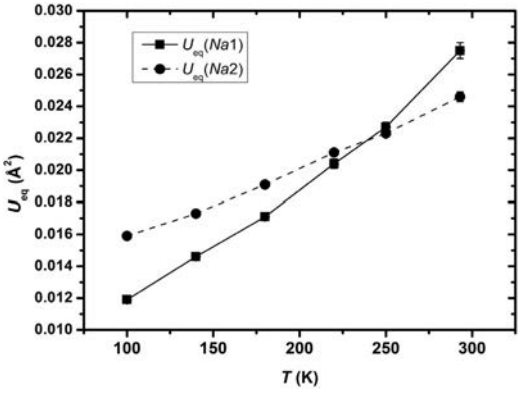

FIG. 8. The variation in the equivalent thermal displacement parameters (U_{eq}) of *Na*1 and *Na*2 as a function of temperature.

possible combinations for couples between successive units: *C*1−*C*1, *C*2−*C*2 and *C*1−*C*2. For the first two of these, the C−C distance is *c*/2 (2.56(2) Å at room-*T*); for the last combination, the C−C distance is 3.81(2) Å at room-*T*. As a consequence, there are three possible configurations of the *Na*2 coordination shells. However, the chemical analyses of cancrinite and the refined site occupancies suggest that vacancies are present at the sites, and these lead to different polyhedral configurations with lower coordination numbers. The absence of superstructures suggests that these vacancies are randomly distributed. The structure refinements show a shortening of the *Na*2−*O*1, *Na*2−*O*3′, *Na*2−*O*4′ and *Na*2−*Oc*1‴ and the stretching of the *Na*2−*O*3″ and *Na*2−*O*4″ bond distances with decreasing temperature (Table 3).

Raman spectra

In the wavenumber range investigated in this study (100−1400 and 3400−3800 cm^{-1}), 29 Raman bands can be distinguished. These are designated ν_1 to ν_{29} with increasing wavenumber and listed in Table 5. A fit with two Lorentzian profiles was used to resolve overlapping peaks. According to previous Raman investigations of open-framework silicates with zeolitic structures (Dutta and Del Barco, 1985; Dutta and Puri, 1987; Lindner *et al.*, 1996; Wopenka *et al.*, 1998; Mozgawa, 2001), the following general mode assignments can be made. The modes between 3400 and 3800 cm^{-1} are caused by O−H stretching of extraframework water molecules. The most intense Raman modes of the carbonate group are usually observed between 700 (in-plane bending mode) and 1100 cm^{-1} (symmetric stretching mode), whereas weak Raman peaks occur near 1400 cm^{-1} due to the asymmetric stretch (Nakamoto *et al.*, 1957; Frost *et al.*, 2009). Other modes between 900 and 1100 cm^{-1} are also assigned to inter-tetrahedral antisymmetric T−O−T (T = Si or Al) stretching vibrations. Inter-tetrahedral symmetric T−O−T stretching vibrations range between 640 and 760 cm^{-1}. Bands below 550 cm^{-1} are assigned to various intra-tetrahedral δ(O−T−O) bending and rotational modes, and to lattice modes. For our cancrinite, the anisotropy of the Raman effect is extremely evident in terms of intensities of the bands, which vary significantly with crystal orientation (Fig. 4).

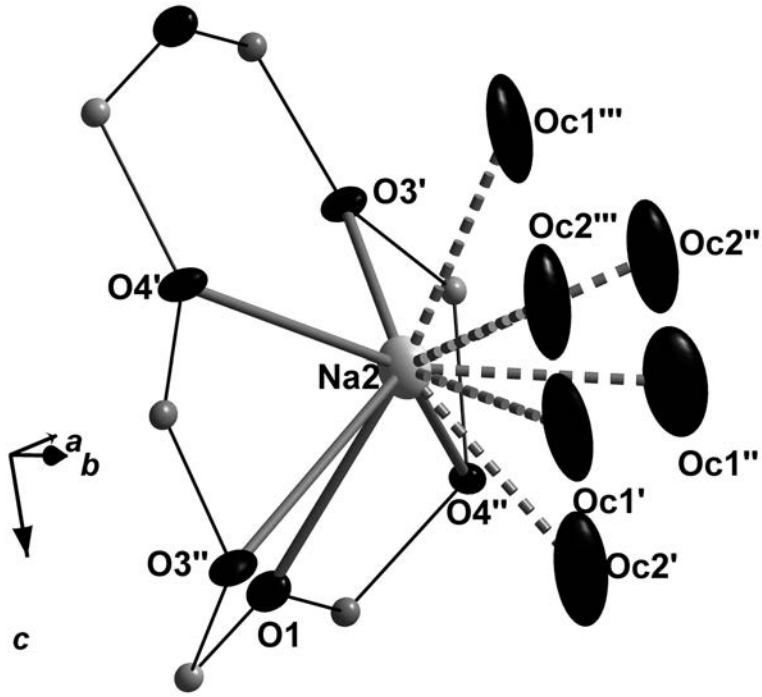

FIG. 9. Coordination shell of the *Na*2 site (5 framework oxygen atoms on one side and up to three carbonate oxygen atoms on the other, maximum CN = 8). Different and mutually exclusive coordination shells are possible (see Table 4).

Discussion

Thermoelastic behaviour

The low number and the scattering of the data prevented an accurate description of the elastic behaviour of natural cancrinite at low temperature. The volume thermal expansion coefficient, α, must be fixed as constant due to the low number of $V-T$ data. The refined α_V, α_a and α_c thermal expansion parameters agree with the corresponding mean thermal expansion parameters (i.e. $\bar{\alpha}_V$, $\bar{\alpha}_a$ and $\bar{\alpha}_c$) to within 1σ. Moreover, no evidence of gas-flux induced dehydration phenomena (Gatta and Lotti, 2011) and no change of the deformation mechanism were detected (see below), suggesting the absence of any kind of phase transition. The volume thermal expansion coefficient obtained in this study is in good agreement with that obtained by Hassan *et al.* (2006) for a natural cancrinite with the formula $Na_{5.96}Ca_{1.52}[Al_6Si_6O_{24}](CO_3)_{1.57}\cdot 1.75H_2O$, in the T-range 298–769 K (i.e. $\alpha_V = 4.2(4)\times 10^{-5}$ K^{-1}).

TABLE 4. Mutually exclusive coordination shells (a, b and c) for the *Na*2 site in the cancrinite structure.

		'a'	'b'	'c'
*Na*2–	*O*1	●	●	●
	*O*3′	●	●	●
	*O*4′	●	●	●
	*O*3″	●	●	●
	*O*4″	●	●	●
	*Oc*1′	●		
	*Oc*1″	●		
	*Oc*1‴	●		●
	*Oc*2′		●	●
	*Oc*2″		●	
	*Oc*2‴		●	

Low-T framework behaviour

The main deformation mechanisms at low-T of the cancrinite framework act through tetrahedral tilting, and in particular by anti-cooperative

TABLE 5. Frequencies of Raman bands of cancrinite at room temperature.

Band	Frequency (cm^{-1})	
ν_1	108	
ν_2	115	
ν_3	161	
ν_4	231	
ν_5	277	
ν_6	293	
ν_7	338	Intra-tetrahedral O−T−O bending and rotational modes, and lattice modes
ν_8	350	
ν_9	364	
ν_{10}	401	
ν_{11}	418	
ν_{12}	440	
ν_{13}	460	
ν_{14}	469	
ν_{15}	499	
ν_{16}	631	Inter-tetrahedral *symmetric* T−O−T stretching modes and in-plane bending modes of CO_3 group
ν_{17}	685	
ν_{18}	768	
ν_{19}	816	
ν_{20}	938	Inter-tetrahedral *antisymmetric* T−O−T stretching modes and symmetric stretching modes of CO_3 group
ν_{21}	960	
ν_{23}	976	
ν_{24}	981	
ν_{25}	1002	
ν_{26}	1042	
ν_{27}	1057	
ν_{28}	3536	O−H stretching modes
ν_{29}	3647	

rotation of adjacent tetrahedra. For a given tetrahedron belonging to a given A plane which shows a clockwise rotation, the four adjacent vertex-sharing tetrahedra (two in the same A plane and two in the next B plane) show an anticlockwise rotation (Figs 1 and 2). This mechanism is responsible for the ditrigonalization process of the 6mR⊥[0001] and for the shortening of the *O*3−*O*4 distance of the 4mR joint units, whereas the ditrigonalization itself gives rise to the shortening of the *O*1−*O*1 distances of the 12mRs. Each pair of tetrahedra associated with the opening of the ω1 angle shares the upward *O*3 and *O*4 apices with the bases of two tetrahedra in the successive plane, which shows in turn an opposite rotation (Fig. 2): this forces the *O*3 and *O*4 apices to move towards each other, with a consequent decrease of the tilting angle between the tetrahedra bases and the (0001) plane and a reduction of the corrugation of the rings.

The contraction in the (0001) plane reflects the shortening along the directions defined by the *O*1−*O*1 distances of 12mRs and *O*3−*O*4 distances of 4mRs (Fig. 2), in response of the ditrigonalization of the 6mR⊥[0001]. The decrease of the corrugation of the rings in the (0001) plane might explain the contraction along the *c* crystallographic direction. Moreover, the flattening of the cancrinite cages, described by the closure of the κ angle (Fig. 2), is also responsible for a contraction along [0001], even though the closure of κ is also controlled by the ditrigonalization of the 6mR⊥[0001]. As no change of <*T*−*O*> bond distances occurs with temperature (Table 3), we consider that the framework tetrahedra act as rigid units within the *T*-range investigated.

Low-T extraframework behaviour

The equivalent displacement parameters of the carbonate group sites are almost constant in the temperature range investigated (Table 3) and, for all of them, the U_{33} parameter has a value that is significantly higher than U_{11} and U_{22} (Fig. 3; and deposited material). This unrealistic configuration can be explained by a positional disorder along [0001] of the *C*1 and *C*2 sites (and the related oxygen sites), maintained at low-*T*. The equivalent displacement parameters of *Na*1 and *Na*2 linearly decrease with temperature, but the trend is steeper for *Na*1 (Fig. 8). This behaviour could be due to a higher positional disorder of the *Na*2 site, which is in some way related to the positional disorder of the carbonate groups along the *c* axis, coupled with the presence of different possible coordination polyhedra (i.e. due to CO_3-group vacancies).

As only the *Na*1 and *Na*2 to framework oxygen bond distances change with temperature, whereas bond distances between the cationic sites and extraframework oxygen atoms do not show significant variations (Table 3), it appears that the low-*T* induced structure behaviour of natural cancrinite is mainly governed by the continuous framework rearrangement.

The chemical formula deduced on the basis of the structure refinement is $Na_{7.26}Ca_{0.65}[Al_6Si_6O_{24}][CO_3]_{1.63}(H_2O)_2$. If this is compared to the chemical formula reported by Della Ventura *et al.* (2009), it has a higher Na content and a correspondingly lower Ca content.

However, the sum of electrons at the extraframework cationic sites is similar, being 92.86 e^- from the structure refinement of this study and 91.09 e^- from the chemical analysis. The higher amount of CO_3 deduced from the structure refinement is partially due to the presence of F (Della Ventura *et al.*, 2011), which was not considered in the refinement. However, the total positive charge of the refined model is 8.56 p.f.u. whereas the total negative charge (framework + extraframework population) is 9.26 p.f.u.. This discrepancy suggests an overestimation of the occupancy factors at the CO_3 sites, probably as a result of the positional disorder of the CO_3 groups coupled with the partial site occupancy (Table 2 and deposited table with the anisotropic displacement parameters).

Raman spectra

The Raman spectra of our natural cancrinite from Cameroun have strong similarities with those reported in the RRUFF database (i.e. RUFF ID: R100110, French River, Ontario, Canada; RRUFF ID: R050352, York River, Dungannon Township, Ontario, Canada) (Downs, 2006). The spectra that we collected have two relatively broad vibrational modes in the O−H stretching region, at 3536 (ν_{28}) and 3647 (ν_{29}) cm^{-1}, respectively (Table 5). A series of intense bands between 938 and 1057 cm^{-1} (ν_{20}−ν_{27}) are assigned to inter-tetrahedral antisymmetric T−O−T stretching vibrations (Table 5). The intense bands at 1042 (ν_{26}) and 1057 cm^{-1} (ν_{27}) (Fig. 4; Table 5) appear not to be ascribable to the symmetric stretching mode of the carbonate group, as they occur in CO_3-free compounds with the CAN topology (e.g. vishnevite, RUFF ID: R061139; davyne, RUFF ID: R060305; Downs, 2006). Inter-tetrahedral symmetric T−O−T stretching vibrations between 630 and 760 cm^{-1}, are represented by only two relatively intense bands (ν_{16}−ν_{18}, Fig. 4; Table 5). One of the most intense bands in the spectrum, which is probably due to the low-energy δ(O−T−O) bending mode, is at 499 cm^{-1} (ν_{15}) (Table 5). Further relatively intense bands are centred at 418 (ν_{11}) and 460 (ν_{13}) cm^{-1}, respectively. These bands might be assignable to δ(O−T−O) bending modes or to 'breathing' vibrations of the 4- and 6-membered rings (Mozgawa, 2001). Some of the most intense Raman bands occur (ν_4−ν_{10}) between 200 and 400 cm^{-1}. The band at 277 cm^{-1} (ν_5) is the most intense band observed in the Raman spectrum shown in Fig. 4. Raman pleochroism is evident, and the band intensities change significantly with crystal orientation (Fig. 4). The pleochroism probably reflects the orientation of 6mR⊥[0001] and their ...ABAB... stacking sequence (Fig. 1).

Conclusions

This is the first investigation of the elastic behaviour and structural evolution of a natural cancrinite at low temperature. No evidence of a phase transition or change of deformational mechanisms was found within the temperature range investigated ($100 < T$ (K) < 293). The structure refinement based on intensity data collected at room temperature after the low-T experiment confirmed that the low-T induced deformation processes are completely reversible.

The extraframework population does not show significant variations at temperatures down to 100 K. The strong positional disorder of the carbonate groups along the c axis persists within the T-range investigated. The structural behaviour of cancrinite at low-T appears to be governed mainly by continuous framework rearrangement through tetrahedral tilting. In particular, the main deformational mechanisms are represented by the ditrigonalization of the 6m⊥[0001], contraction of the 4mR joint units, decrease of ring corrugation in the (0001) plane and the flattening of the cancrinite cages.

If we compare the structural behaviour of cancrinite observed in this study at low-T with our results at high-P (Lotti *et al*., 2012), we can infer that the main deformation mechanisms are identical, though different in magnitude. Similar findings have been reported for other open-framework materials investigated at low-T and high-P (e.g. fibrous zeolites; Gatta, 2005; Gatta *et al*., 2004, 2010).

Acknowledgements

This project was funded by the Italian MIUR grant n. 2008SPZ743. Our reviewers, S. Quartieri, Y. Lee and P. Williams are thanked for their comments on the manuscript. This paper is dedicated to Mark Welch, in recognition of his important contributions to mineral physics.

References

Baerlocher, C., McCusker, L.B. and Olson, D.H. (2007) *Atlas of Zeolite Framework types*, sixth edition.

Elsevier, Amsterdam.

Ballirano, P. and Maras, A. (2005) The crystal structure of a "disordered" cancrinite. *European Journal of Mineralogy*, **16**, 135–141.

Barnes, M.C., Addai-Mensah, J. and Gerson, A.R. (1999) The mechanism of the sodalite-to-cancrinite phase transformation in synthetic spent Bayer liquor. *Microporous and Mesoporous Materials*, **31**, 287–302.

Bickmore, B.R., Nagy, K.L., Young, J.S. and Drexler, J.W. (2001) Nitrate-cancrinite precipitation on quartz sand in simulated Hanford tank solutions. *Environmental Science and Technology*, **35**, 4481–4486.

Bonaccorsi, E. and Merlino, S. (2005) Modular microporous minerals: cancrinite-davyne group and C–S–H phases. Pp. 241–290 in: *Micro- and Mesoporous Mineral Phases* (G. Ferraris and S. Merlino, editors). Reviews in Mineralogy and Geochemistry, **57**. Mineralogical Society of America, Washington DC and the Geochemical Society, St Louis, Missouri, USA.

Bonaccorsi, E., Della Ventura, G., Bellatreccia, F. and Merlino, S. (2007) The thermal behaviour and dehydration of pitiglianoite, a mineral of the cancrinite-group. *Microporous and Mesoporous Materials*, **99**, 225–235.

Bresciani-Pahor, N., Calligaris, M., Nardin, G. and Randaccio, L. (1982) Structure of a basic cancrinite. *Acta Crystallographica*, **B38**, 893–895.

Brigatti, M.F. and Guggenheim, S. (2002) Mica crystal chemistry and the influence of pressure, temperature, and solid solution on atomistic models. Pp. 1–98 in: *Micas: Crystal Chemistry & Metamorphic Petrology* (A. Mottana, F.P. Sassi, J.B. Thompson Jr and S. Guggenheim, editors) Reviews in Mineralogy and Geochemistry, **46**. Mineralogical Society of America, Washington, DC and the Geochemical Society, St Louis, Missouri, USA.

Brown, W.L. and Cesbron, F. (1973) Sur les surstructures des cancrinites. *Comptes Rendus de l'Academie de Sciences*, **276 (Aer. D)**, 1–4.

Buck, E.C. and McNamara, B.K. (2004) Precipitation of nitrate-cancrinite in Hanford tank sludge. *Environmental Science and Technology*, **38**, 4432–4438.

Buhl, J.C., Stief, F., Fechtelkord, M., Gesing, T.M., Taphorn, U. and Taake, C. (2000) Synthesis, X-ray diffraction and MAS NMR characteristics of nitrate cancrinite $Na_{7.6}[AlSiO_4]_6(NO_3)_{1.6}(H_2O)_2$. *Journal of Alloys and Compounds*, **305**, 93–102.

Cámara, F., Bellatreccia, F., Della Ventura, G. and Mottana, A. (2005) Farneseite, a new mineral of the cancrinite-sodalite group with a 14 layer stacking sequence: occurrence and crystal structure. *European Journal of Mineralogy*, **17**, 839–846.

Cámara, F., Bellatreccia, F., Della Ventura, G., Mottana, A., Bindi, L., Gunter, M.E. and Sebastiani, M. (2010) Fantappièite, a new mineral of the cancrinite-sodalite group with a 33-layer stacking sequence: occurrence and crystal structure. *American Mineralogist*, **95**, 472–480.

Della Ventura, G., Bellatreccia, F., Parodi, G.C., Cámara, F. and Piccinini, M. (2007) Single-crystal FTIR and X-ray study of vishnevite, ideally $[Na_6(SO_4)][Na_2(H_2O)_2](Si_6Al_6O_{24})$. *American Mineralogist*, **92**, 713–721.

Della Ventura, G., Gatta, G.D., Redhammer, G.J., Bellatreccia, F., Loose, A. and Parodi, G.C. (2009) Single-crystal polarized FTIR spectroscopy and neutron diffraction refinement of cancrinite. *Physics and Chemistry of Minerals*, **36**, 193–206.

Downs, R.T. (2006) RRUFF database. *Program and Abstracts of the 19th General Meeting of the International Mineralogical Association*, Kobe, Japan, O03–13.

Dutta, P.K. and Del Barco, B. (1985) Structure-sensitive Raman bands in hydrated zeolite A. *Journal of the Chemical Society, Chemical Communications*, **1985**, 1297–1299.

Dutta, P.K. and Puri, M. (1987) Synthesis and structure of zeolite ZSM-5 – a Raman-spectroscopic study. *Journal of Physical Chemistry*, **91**, 4329–4333.

Fechtelkord, M., Stief, F. and Buhl, J.C. (2001) Sodium cation dynamics in nitrate cancrinite: a low and high temperature ^{23}Na and ^{1}H MAS NMR study and high temperature Rietveld structure refinement. *American Mineralogist*, **86**, 165–175.

Foit, F.F. Jr, Peacor, D.R. and Heinrich, E.W.M. (1973) Cancrinite with a new superstructure from Bancroft, Ontario. *The Canadian Mineralogist*, **11**, 940–951.

Frost, R.L., Bahfenne, S. and Graham, J.E. (2009) A Raman spectroscopic study of the antimony mineral klebelsbergite $Sb_4O_4(OH)_2(SO_4)$. *Journal of Raman Spectroscopy*, **40**, 855–860.

Gatta, G.D. (2005) A comparative study of fibrous zeolites under pressure. *European Journal of Mineralogy*, **17**, 411–421.

Gatta G.D. and Lee Y. (2008) Pressure-induced structural evolution and elastic behaviour of $Na_6Cs_2Ga_6Ge_6O_{24}{\cdot}Ge(OH)_6$ variant of cancrinite: a synchrotron powder diffraction study. *Microporous and Mesoporous Materials*, **116**, 51–58

Gatta, G.D. and Lotti, P. (2011) On the low-temperature behavior of the zeolite gobbinsite: a single-crystal X-ray diffraction study. *Microporous and Mesoporous Materials*, **143**, 467–476.

Gatta, G.D., Boffa Ballaran, T., Comodi, P. and Zanazzi, P.F. (2004) Comparative compressibility and equation of state of orthorhombic and tetragonal edingtonite. *Physics and Chemistry of Minerals*, **31**, 288–298.

Gatta, G.D., Kahlenberg, V., Kaindl, R., Rotiroti, N., Cappelletti, P. and de' Gennaro, M. (2010) Crystal-structure and low-temperature behavior of "disordered" thomsonite. *American Mineralogist*, **95**, 495–502.

Gerson, A.R. and Zheng, K. (1997) Bayer process plant scale: transformation of sodalite to cancrinite. *Journal of Crystal Growth*, **171**, 209–218.

Grundy, H.D. and Hassan, I. (1982) The crystal structure of a carbonate-rich cancrinite. *The Canadian Mineralogist*, **20**, 239–251.

Hassan, I. and Buseck, P.R. (1992) The origin of the superstructure and modulations in cancrinite. *The Canadian Mineralogist*, **30**, 49–59.

Hassan, I. and Grundy, H.D. (1984) The character of the cancrinite–vishnevite solid solution series. *The Canadian Mineralogist*, **22**, 333–340.

Hassan, I. and Grundy, H.D. (1991) The crystal structure of basic cancrinite, ideally $Na_8[Al_6Si_6O_{24}](OH)_2{\cdot}3H_2O$. *The Canadian Mineralogist*, **29**, 377–383.

Hassan, I., Antao, S.M. and Parise, J.B. (2006) Cancrinite: crystal structure, phase transitions, and dehydration behavior with temperature. *American Mineralogist*, **91**, 1117–1124.

Isupova, D., Ida, A., Kihara, K., Morishita, T. and Bulka, G. (2010) Asymmetric thermal vibrations of atoms and pyroelectricity in cancrinite. *Journal of Mineralogical and Petrological Sciences*, **105**, 29–41.

Jarchow, O. (1965) Atomanordnung und strukturverfeinerung von Cancrinit. *Zeitschrift für Kristallografie*, **122**, 407–422.

Lindner, G.G., Hoffmann, K., Witke, K., Reinen, D., Heinemann, C. and Koch, W. (1996) Spectroscopic properties of Se-2(2-) and Se-2(-) in cancrinite. *Journal of Solid State Chemistry*, **126**, 50–54.

Lotti, P., Gatta, G.D., Rotiroti, N. and Cámara, F. (2012) High-pressure study of a natural cancrinite. *American Mineralogist*, **97**, 872–882.

McCusker, L.B., Liebau, F. and Engelhardt, G. (2001) Nomenclature of structural and compositional characteristics of ordered microporous and mesoporous materials with inorganic hosts. *Pure and Applied Chemistry*, **73**, 381–394.

Mozgawa, W. (2001) The relation between structure and vibrational spectra of natural zeolites. *Journal of Molecular Structure*, **596**, 129–137.

Nakamoto, K., Fujita, J., Tanaka, S. and Kobayashi, M. (1957) Infrared spectra of metallic complexes IV. Comparison of the infrared spectra of unidentate and bidentate metallic complexes. *Journal of the American Chemical Society*, **79**, 4904–4908.

Oxford Diffraction (2008) *Xcalibur CCD System, CrysAlis Software System*. Oxford Diffraction Ltd, Oxford, UK.

Pauling, L. (1930) The structure of some sodium and calcium aluminosilicates. *Proceedings of the National Academy of Sciences*, **16**, 453–459.

Poborchii, V.V. (1994) Structure of one-dimensional selenium chains in zeolite channels by polarized Raman scattering. *Journal of Physics and Chemistry of Solids*, **55**, 737–774.

Poborchii, V.V., Lindner, G.G. and Sato, M. (2002) Selenium dimers and linear chains in one-dimensional cancrinite nanochannels: structure, dynamics, and optical properties. *Journal of Chemical Physics*, **116**, 2609–2617.

Rastvetaeva, R., Pekov, I., Chukanov, N., Rozenberg, K. and Olysych, L. (2007) Crystal structures of low-symmetry cancrinite and cancrisilite varieties. *Crystallography Reports*, **52**, 811–818.

Sheldrick, G.M. (1997) *SHELX-97 – A program for crystal structure refinement*. University of Göttingen, Göttingen, Germany.

Wilson, A.J.C. and Prince, E. (1999) *International Tables for Crystallography Vol. C, Mathematical, Physical and Chemical tables*, second edition. Kluwer, Dordrecht, The Netherlands.

Wopenka, B., Freeman, J.J. and Nikisher, T. (1998) Raman spectroscopic identification of fibrous natural zeolites. *Applied Spectroscopy*, **52**, 54–63.

Zhao, H., Deng, Y., Harsh, J.B., Flury, M. and Boyle, J.S. (2004) Alteration of kaolinite to cancrinite and sodalite by simulated Hanford tank waste and its impact on cesium retention. *Clays and Clay Minerals*, **52**, 1–13.